J. Fluid Mech. (1988), 190, *vol. pp.* 241–263
Printed in Great Britain

Turbulent structure in low-concentration drag-reducing channel flows

By T. S. LUCHIK† AND W. G. TIEDERMAN‡

† Jet Propulsion Laboratory, California Institute of Technology, Pasadena, CA 91109, USA
‡ School of Mechanical Engineering, Purdue University, West Lafayette, IN 47907, USA

(Received 7 January 1986 and in revised form 19 October 1987)

A two-component laser-Doppler velocimeter was used to measure simultaneously velocity components parallel and normal to the wall in two fully developed, well-mixed, low-concentration (1–2 p.p.m.) drag-reducing channel flows and one turbulent channel flow of water. The mean velocity profiles, root-mean-square velocity profiles and the distributions of the $\overline{uv}$ turbulent correlation confirm that the additives modify the buffer region of the flow. The principal influence of the additives is to damp velocity fluctuations normal to the wall in the buffer region.

The structural results show that the average time between bursts increased for the drag-reducing flows. When compared to a water flow at the same wall shear stress, this increase in the timescale was equal to the increase in the average streak spacing. Conditionally averaged velocity signals of $y^+ = 30$ centred on the leading edge of a burst, as well as those centred on the trailing edge, have the same general characteristics in all three flows indicating that the basic structure of the fundamental momentum transport event is the same in these drag-reducing flows. However, it was clearly shown that the lower-threshold Reynolds-stress-producing motions were damped while the higher-threshold motions were not damped. In the buffer region of the drag-reducing flows this yields a larger mean velocity gradient with damped fluctuations normal to the wall and increased fluctuations in the streamwise direction. It is hypothesized that some strong turbulent motions are required to maintain extended polymer molecules, which produce a solution with properties that can damp lower threshold turbulence and thereby reduce viscous drag.

1. Introduction

The addition of soluble, high-molecular-weight polymer molecules to turbulent liquid flows has been one of the most successful methods for reducing drag. There are two techniques that have been successful. In one case, polymer solutions with concentrations of the order of several thousand p.p.m. are injected either along the centreline of a pipe flow (Bewersdorff 1985; Berman 1986) or at the wall (Frings 1985). In these flows a good portion, if not all, of the polymer solution remains unmixed or breaks up into threads of concentrated polymer solution that may be dispersed throughout the flow field. This relatively new technique differs significantly from the original (dilute solution) technique where polymer solutions with concentrations of the order of several hundred p.p.m. or less were used and the solutions mixed with the solvent at the molecular level. This paper considers only the latter case where there is no evidence of an unmixed layer or threads of concentrated polymer solution.

Wells & Spangler (1967) and Wu & Tulin (1972) showed that the flow must be

turbulent and the additives must be in the wall region in order for dilute polymer solutions to reduce the wall shear stress. The effective region for the additives was further defined by Reischman & Tiederman (1975) who showed that the polymer solutions had their largest effect on the mean velocity profile in the buffer region ($10 < y^+ < 100$).† McComb & Rabie (1982) observed similar changes in the mean velocity profile and with concentration measurements established that the buffer region is the only portion of the flow where the polymer molecules must be in order to reduce drag. Tiederman, Luchik & Bogard (1985) also demonstrated that the polymer additive is not effective when it is confined to the linear sublayer.

Walker, Tiederman & Luchik (1986) attempted to take advantage of this knowledge about the region where the polymer molecules are effective in an experimental study designed to optimize the additive injection process for channel flows. Using flush-mounted injectors, Walker *et al.* (1986) found that drag reduction peaked about 10 channel heights downstream of the injection slot. The wall-layer polymer concentration in the vicinity of this peak in drag reduction was nearly one order of magnitude larger than the fully mixed concentration, showing that there were appreciable concentration gradients normal to the wall at this streamwise location. Walker *et al.* also showed that for distances greater than 30 channel heights downstream of the injection slot, drag reduction was nearly constant and the polymer concentration was equal to the fully mixed polymer concentration.

Results from the fully mixed region of Walker *et al.* (1986) motivated this study because drag reductions of 20 to 30% were achieved with polymer concentrations of only 1 to 3 p.p.m. These are ideal drag-reducing flows to investigate because the flow is fully developed, the differences in the rheological properties of the drag-reducing solution and solvent are minimal and significant drag reduction is occurring.

The important issues are how these low-concentration polymer solutions alter the turbulent flow field and cause drag to be reduced. In this study, both the time-averaged character of the streamwise and normal velocity components as well as time-averaged and conditionally averaged properties of the coherent wall-layer structure were deduced from two-component laser-velocimeter measurements.

Most velocity measurements in turbulent drag-reducing flows have been single-component measurements of the streamwise velocity component in flows where the polymer concentration was about 50 to 100 p.p.m. (McComb & Rabie 1982; Reischman & Tiederman 1975). These measurements have shown an increase in the thickness of the buffer region and an increase in the peak value of the root mean square (r.m.s.) of the streamwise velocity component. This peak is broader in extent and located farther from the wall in drag-reducing flows than in water flows. The first objective of the present study was to obtain a more detailed description of the time-averaged flow field in a low-concentration drag-reducing flow and compare those results with those of a water flow. The flow quantities of particular interest were the r.m.s. of the normal velocity component, v', and the $\overline{uv}$ turbulent correlation. Here u and v are the fluctuating velocities in the streamwise and normal directions. These flow quantities give the best indication of how the drag-reducing additives alter the time-average turbulent transport normal to the wall.

The portion of the study related to the coherent wall-layer structure was motivated by the experiments of Kim, Kline & Reynolds (1971) and Corino & Brodkey (1969) who found that essentially all of the turbulent kinetic energy and

† The distance from the wall, y, has been normalized with the wall shear velocity, $u_\tau = (\tau_w/\rho)^{\frac{1}{2}}$ and the kinematic viscosity ν. Here τ_w is the wall shear stress and ρ is the fluid density.

most of the turbulent transport occurs during burst events associated with this structure. The burst event is a sudden outrush of low-momentum fluid away from the wall. Associated with each burst is a sweep or inrush of high-momentum fluid toward the wall. Since there are large variations in the velocity field in the near-wall region during a burst event and since drag-reducing solutions have an effect on the time-averaged flow field in the same region, the changes that take place in the burst events in drag-reducing flows are of particular interest.

The burst event includes the ejection and breakup of all or part of a wall-layer streak which is a long, narrow region of low-speed fluid very near the wall ($y^+ \leqslant 5$). Streaks remain stable for some streamwise distance, lift away from the wall, and break up by ejecting low-momentum fluid away from the wall. Within the burst there are one or more coherent filaments of low-momentum fluid which move away from the wall and are called ejections. The burst event occurs in a quasi-periodic manner. Therefore, experimentalists have concentrated their efforts on measuring statistical quantities such as the average time between bursts and the average spanwise spacing of the streaks.

There have been previous studies of these coherent structures in drag-reducing flows where the polymer concentration was 50 p.p.m. or higher. Oldaker & Tiederman (1977) showed that the average non-dimensional spacing between streaks, λ^+, increases linearly with increasing drag reduction for fully mixed drag-reducing flows. They also noted that the viscous sublayer was more stable when polymer solutions were present. Donohue, Tiederman & Reischman (1972), Achia & Thompson (1977) and Tiederman, Smith & Oldaker (1977) all reported that the ratio of the average time between bursts for a drag-reducing flow and a water flow at the same shear stress was equal to the ratio of the streak spacings for the two flows. This led those authors to the conclusion that the burst event was not directly affected by the drag-reducing solutions. However, as discussed by Bogard & Tiederman (1983) these earlier methods for deducing the time between bursts were not accurate because not all of the events within the field of view were marked and counted. Using more accurate methods, Tiederman *et al.* (1985) as well as Walker *et al.* (1986) showed that the burst rate decreased more than the increase in streak spacing at streamwise locations near the wall injection of 100, 200 and 700 p.p.m. polymer solutions. Since there were large gradients of additive concentration normal to the wall at the streamwise location of these measurements, it is possible that the turbulence production and drag-reducing mechanisms were not in an equilibrium state. However, similar results for burst rates in homogeneous flows were obtained by McComb & Rabie (1982) using the autocorrelation of the streamwise velocity component.

Although the flow-visualization technique used by Tiederman *et al.* (1985) yields accurate values for the average time between bursts, it is not a practical technique for obtaining statistical velocity quantities based on conditional sampling. Consequently, the modified u-level technique of Luchik & Tiederman (1987) was used to detect the burst and ejection structures. This technique uses the concept of grouping ejections into burst structures (see Bogard & Tiederman 1986) and it has been verified by comparing both the average time between bursts and the conditionally averaged velocity signals associated with ejections with the burst periods and signals obtained by Bogard (1982) when flow visualization was the detector.

The principal experimental devices were a three-beam, two-colour laser velocimeter and a long, two-dimensional channel, described in the next section. Discussion

of the results will be divided into two parts. The first will centre on the time-averaged statistics of the velocity field while the second will present a comparison of the burst structures.

2. Apparatus and procedure

2.1. *Flow loop*

The experiments were performed in a recirculating-flow loop with a rectangular cross-section test section. Upstream of the test section was a large stilling tank which contained a perforated plate, a screen–sponge–screen section and a series of two two-dimensional nozzles which reduced the flow area to 2.5×25 cm. The flow then passed through a section of closely packed 5.6 mm i.d. plastic tubes. With these provisions, the flow entered the test section without any large-scale vorticity. At the downstream end of the test section, a large stilling tank with a cooling coil for temperature control provided damping of disturbances created from the outlet.

The two-dimensional-flow channel had an internal cross-section of 2.5×25.0 cm. Located in the channel were a pair of polymer injection slots and a thin (0.127 mm wide) slot used for flow visualization. The polymer injection slots spanned the centre 22.5 cm of the channel walls and were located 60 channel heights downstream of the channel inlet and 136 channel heights upstream of the outlet. These slots made an angle of 25° with the main flow direction and were 0.13 cm wide. The flow-visualization slot was 123 channel heights downstream of the channel inlet and was used to mark ejection and burst structures. Velocity profiles were measured more than 65 channel heights downstream of the polymer injection slots where the injected solutions had become fully mixed with the channel flow of water (see Walker *et al.* 1986). Polymer solutions flowed by gravity from an overhead reservoir to the injection slots. The flow to each slot was regulated by a separate rotameter and flow control valve.

The bottom plate of the test section had a line of pressure tape to monitor the local pressure gradient. Two micrometer manometers with carbon tetrachloride as the manometer fluid were used to measure the pressure drop. With this manometer fluid, pressure-drop measurements could be made with a sensitivity of 0.015 mm of water.

2.2. *Experimental technique*

Prior to each experiment, filtered and softened tap water was deaerated by heating it to 50 °C in a separate holding tank and then allowing it to cool to room temperature. The water temperature in the channel was held constant at 24 °C during an experiment.

The drag-reducing additives were solutions of SEPARAN AP-273, a polyacrylamide manufactured by Dow Chemical Corp., with filtered tap water as the solvent. The polymer solutions were initially mixed to 2560 p.p.m. and 2920 p.p.m. These concentrated mixtures were allowed to hydrate for 12–24 hours prior to dilution to 400 p.p.m. and 700 p.p.m., respectively.

In order to avoid using solutions with significant batch-to-batch variations, the drag-reducing capability of each polymer solution was required to yield 'standard values' in a 14.05 mm i.d. tube. The polymer solutions were also checked for consistency by measuring the viscosity of the solutions at shear rates of 115 s^{-1} and 230 s^{-1} using a Wells-Brookfield LVT-SCP 1.565° cone-and-plate viscometer.

During an experiment, the amount of drag reduction was deduced from pressure-drop measurements. For fully developed flow, the pressure gradient is proportional

to the wall shear stress, and the viscous drag. By assuming that the flow is two-dimensional and fully developed, which are good assumptions in the vicinity of the measurement location, drag reduction was calculated using

$$D_R = \frac{\Delta P - \Delta P_i}{\Delta P}. \tag{2.1}$$

Here, ΔP is the water-flow pressure drop and ΔP_i is the pressure drop with polymer solution present in the flow. Because the fluid is recirculated with intermittent injection of polymer, the water-flow pressure gradient had to be monitored periodically during an experiment to ensure that drag reduction due to polymer build-up in the channel did not occur. These checks showed that once the polymer solution had passed the test section, it was no longer an effective drag reducer. It is hypothesized that the polymer molecules were degraded by the high shears in the centrifugal pump and orifice.

2.3. *Flow visualization*

Ejections were marked by seeping fluid dyed with 2 g/l fluorescein disodium salt through the small 0.127 mm wide flow-visualization slot. The dye-marked wall structure was illuminated and recorded using a Video Logic Corp. INSTAR IV high-speed motion analyser. The system records 120 frames per s on 1 in. video tape using a synchronous strobe to give an exposure time of 10 μs. Flow-visualization data were used for two purposes: first to yield qualitative information from which original hypotheses were formed, and second to deduce the average ejection period directly and the average burst period assuming two ejections per burst for the water flow (Bogard & Tiederman 1983; Offen & Kline 1975). However, the average number of ejections per burst for the low-concentration flows was unknown. It was determined by simultaneous visualization of one streak and the number of ejections resulting from each streak instability. This was done at Reynolds numbers of 17800 with 25% drag reduction and 15800 with 20% drag reduction. In all cases the Reynolds number is based on the mass average velocity U_m and the channel height h. These visualization results showed that 2.4 ejections per burst occurred on average for both flow conditions and this value was used to reduce all of the drag-reducing flow-visualization data in this study. This result is significantly different from the 3.5 ejections per burst measured by Luchik & Tiederman (1984) in a region where significant polymer concentration gradients were present and where the time-average wall-layer concentration of about 50 p.p.m. was decreasing with streamwise direction due to mixing.

The data for the average time between bursts obtained from flow visualization was used as a standard to which the values obtained using the modified u-level technique were compared.

2.4. *Laser velocimeter*

Velocity measurements were made using a three-beam, two-component TSI model 9100-8 laser-Doppler velocimeter. The system included frequency shifting at 40 MHz with electronic down mixing, 2.27 beam expansion and dual aperture collection (to minimize optical noise and allow finer focusing on the probe volume). To eliminate fringe wash-out due to unequal optical path lengths of the three beams, a path length compensator, consisting of 50.8 mm long piece of optical-quality glass, was placed in the path of the blue–green beam downstream of the colour separator and upstream of the beam expander. Scattered light was collected in the forward direction. Parameters for the velocimeter are summarized in table 1.

	Blue	Green
Probe-volume length (mm)	1.0214	1.080
Probe-volume diameter (μm)	52.4	55.2
Fringe spacing (μm)	3.402	3.624
Effective frequency shift (MHz)	−1.0	+1.0
Beam spacing (mm)	35.3	35.3

TABLE 1. Laser-velocimeter parameters

The photomultiplier output was processed using TSI model 1980 counter-type processors. Each processor was operated in the N-cycle mode with $N = 8$ fringes. Only one data point was taken per Doppler burst and a coincidence window was imposed on the two outputs. The maximum allowable time for coincidence was calculated by dividing the probe-volume diameter by the highest velocity expected in the channel.

The data-collection electronics included a DEC PDP 11/03 minicomputer and TSI model 1998 interfaces. Data were stored temporarily on a floppy disk prior to being transferred to a VAX 11/780 for initial data reduction. Data were then transferred to CDC 6500 and 6600 computers for further analysis and permanent storage.

The velocity data were taken at angles of $\pm 45°$ to the main flow direction so that the three-beam system could be traversed as close to the wall as possible. The direct measurements were decomposed into streamwise and normal velocity components using a standard rotation of axes such that

$$U_i = 0.7071[U_i|_{+45} + U_i|_{-45}], \tag{2.2}$$

$$V_i = 0.7071[U_i|_{+45} - U_i|_{-45}], \tag{2.3}$$

where U_i with the subscript ± 45 are the measured velocities at $\pm 45°$ to the main flow direction, U_i without any additional subscript is the instantaneous streamwise velocity component and V_i is the instantaneous normal velocity component. This arrangement has the advantage of allowing measurements close to a wall. The disadvantage is that the normal velocity component is proportional to the difference of two numbers of nearly the same magnitude. To overcome this disadvantage the components at $\pm 45°$ must be measured with good resolution.

Movement of the probe volume normal to the wall was accomplished using a traversing system that had a range of 25.4 mm. A position could be located with an accuracy of ± 0.013 mm with this system.

Different methods were used to acquire velocity data for the long-time-averaged flow characteristics and the conditionally averaged signals of the burst structures. The data for the long-time-averaged flow characteristics were taken at a sampling rate of 50 Hz with a particle arrival rate in excess of 3000 Hz. Using this type of sampling technique, velocity bias is eliminated as shown by Stevenson, Thompson & Roesler (1982) and Luchik (1982). Ensembles of 5000 samples per component were used to make initial estimates of the mean and r.m.s. velocities. New estimates of the long-time-averaged quantities were calculated using only velocity realizations within four standard deviations of the respective mean. This procedure generally discarded less than 15 samples of either the streamwise or the normal velocity component.

The velocity data for the conditionally averaged signals were taken as fast as possible; generally the rate was greater than 2000 Hz. The time between adjacent

	Water	Equal-Reynolds-number drag-reducing flow	Equal-wall-shear drag-reducing flow
Re_h	17800	17800	22000
U_m (m/s)	0.646	0.647	0.799
U_0 (m/s)	0.782	0.776	0.936
u_τ (cm/s)	3.77	3.33	3.77
$\nu \times 10^{+6}$ (m^2/s)	0.907	0.907	0.907
D_R (%)	—	22	31
C (p.p.m.)	—	1.3	2.1

TABLE 2. Experimental conditions

data points was also recorded. These data were used to reconstruct the time-resolved velocity signal. This signal was then sampled at a rate equal to the viscous frequency (u_τ^2/ν). This procedure was used because the method of Stevenson *et al.* (1982) requires a 10 to 1 ratio between the particle arrival rate and the sampling rate to remove velocity bias. This criterion could not be met when it was necessary to sample at the viscous frequency. Because of the data storage limitation of the PDP minicomputer, multiple velocity records were taken at this fast rate so that the total sampling time was greater than 400 burst periods. For the two-component measurements, 50–60% of the data verified by either processor also met the requirement imposed by the coincidence window.

2.5. *Experimental conditions*

Three flows were studied. The baseline flow was a fully developed water flow. Two drag-reducing flows were compared to this baseline flow. For one, the Reynolds number was matched, and for the second, the wall shear stress of the water flow was matched. The experimental conditions summarized in table 2 show that the fully mixed polymer concentration, C, for the drag reducing flows was only 1.3 and 2.1 p.p.m. A 50 μs and 70 μs coincidence window was used for $Re_h = 22000$ and $Re_h = 17800$, respectively.

3. Time-average results

Since this paper is concerned primarily with the effects of drag-reducing additives on fully developed turbulent flow, no comparisons of the present water data with other Newtonian data are presented here. Comparisons were made by Luchik (1985) that show the present water data to compare well with the two-component hot-wire data of Bogard (1982) and Johansson & Alfredsson (1983), as well as the single-component laser-velocimeter data of Luchik & Tiederman (1985), and the miniature hot-wire data of Willmarth & Sharma (1984).

Figure 1 shows the mean streamwise velocity profiles for the water flow, the drag-reducing flow that matches the Reynolds number of the water flow (case ERN) and the drag-reducing flow that matches the wall shear stress of the water flow (case EWS). The drag-reducing data shown in figure 1 are in good qualitative agreement with the data of Reischman & Tiederman (1975) whose experiments were conducted with AP-273 concentrations of 100 p.p.m. When drag-reducing additives are present the buffer region thickens resulting in an additive offset in the logarithmic overlap region. The amount of offset in the present drag-reducing flows is less than the

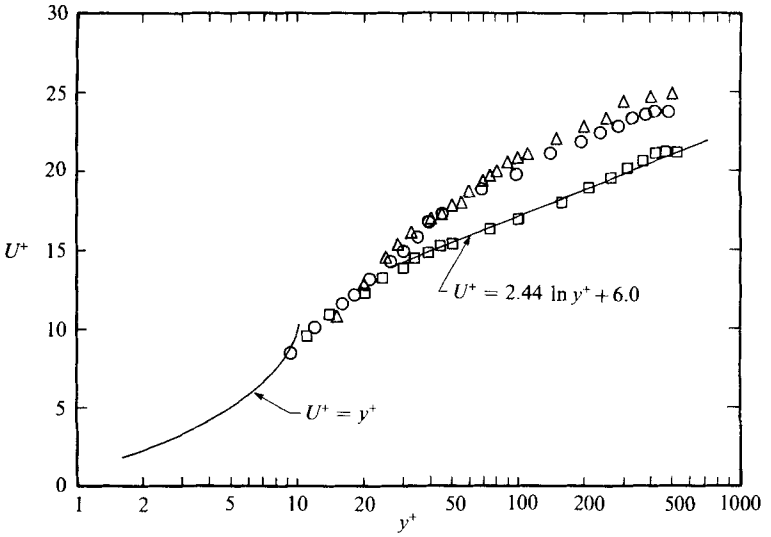

FIGURE 1. Mean velocity profiles: □, water; ○, ERN drag-reducing flow; △, EWS drag-reducing flow.

amount extrapolated on the basis of percentage drag reduction from the experiments of Reischman & Tiederman (1975). This difference in the additive constant ΔB is probably due to differences in the rheological properties of the 100 p.p.m. solutions used by Reischman & Tiederman and the 1–2 p.p.m. solutions used in the present study.

Since it is not yet possible to predict the amount of drag reduction that will occur when polymer molecules are added to a Newtonian flow, a universal method for comparing Newtonian and drag-reducing results is not available. In this study, the centreline velocity U_0 will be used to normalize and compare results from flows at equal Reynolds number while the wall shear velocity u_τ will be used in the comparison of flows at equal wall shear stress. These comparisons have the advantage that any differences can be attributed directly to changes in the numerator of the non-dimensional velocity.

Figure 2 shows the root mean square (r.m.s.) of the streamwise velocity component u' for the two equal-Reynolds-number flows non-dimensionalized with outer variables (a = channel half-height, U_0 = centreline mean velocity). Comparison of the water data with that of the drag-reducing flow shows that the peak in u' broadens as well as moves away from the wall when drag reduction occurs. Note that the peak level of u'/U_0 for these equal-Reynolds-number flows has the same value.

Figure 3 compares levels of u' normalized with inner variables u_τ and ν for the equal-wall-shear cases. Comparison of the water flow to the drag-reducing flow shows only slightly higher levels of u'/u_τ and a broader region over which peak levels occur for the drag-reducing flow. The location of the peak also moves from $y^+ = 15$ for the water flow to $y^+ \approx 30$ for the drag-reducing flows. Trends in these low-polymer-concentration data are in agreement with those for higher-concentration data of Logan (1972), Reischman & Tiederman (1975) and McComb & Rabie (1982). However, the peak value of u'/u_τ for the higher-concentration drag-reducing flows was considerably higher than that for a water flow with equal wall shear stress whereas the present results show a peak in u'/u_τ that is approximately equal to that of a water flow at equal wall shear stress.

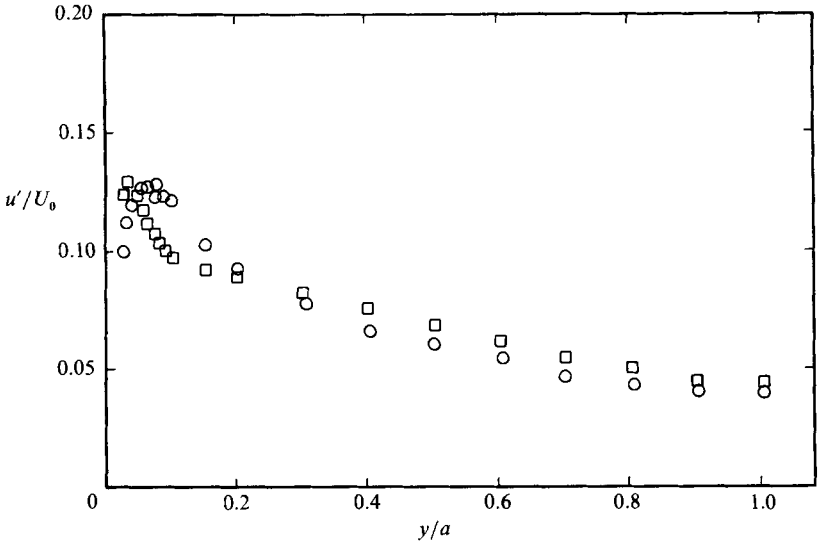

FIGURE 2. Comparison of root mean square of axial velocity fluctuations: □, water; ○, ERN drag-reducing flow.

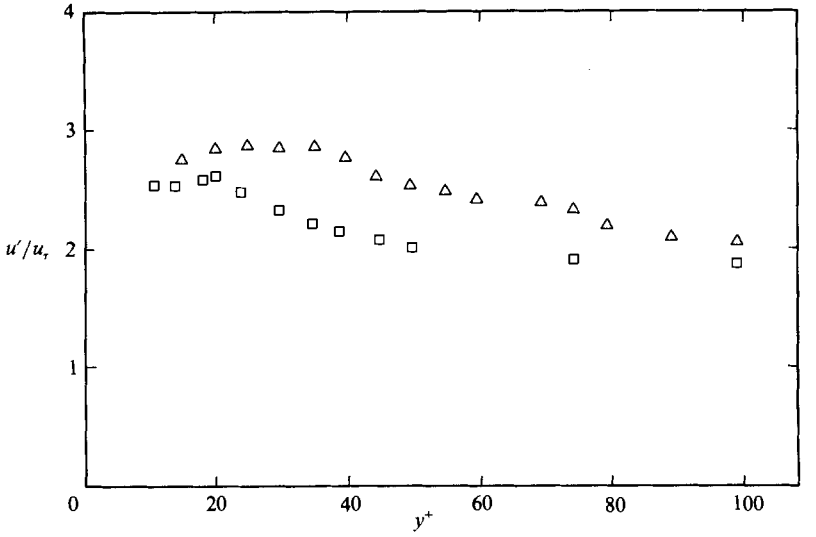

FIGURE 3. Comparison of root mean square of axial velocity fluctuations: □, water; △, EWS drag-reducing flow.

The r.m.s. of the velocity component normal to the wall v' non-dimensionalized with outer variables for the equal-Reynolds-number flows is shown in figure 4. Although the shape of the profile of v'/U_0 is similar in both flows, there is considerable damping of v' throughout the drag-reducing flow field, even at the centreline where the drag-reducing solutions had minimal effects on $\bar{U}$ and u'.

Values of v' normalized with inner variables for the equal-wall-shear flows are shown in figure 5. Damping of the fluid movement normal to the wall in the drag-reducing flow occurs throughout the buffer region. However, the most appreciable damping, about 5%, occurs in the thickened portion of the buffer region. Also a nearly constant level of v' occurred across the buffer region of the flow. In contrast

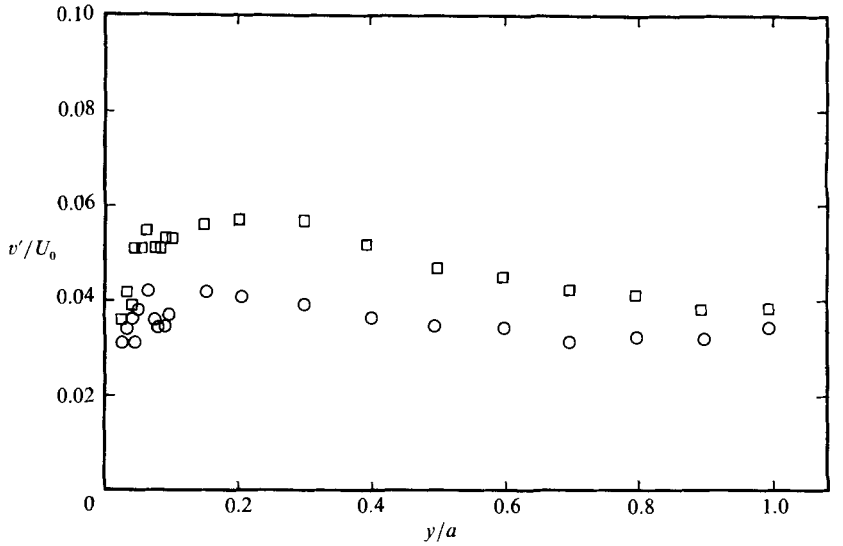

FIGURE 4. Comparison of root mean square of velocity fluctuations normal to wall: □, water; ○, ERN drag-reducing flow.

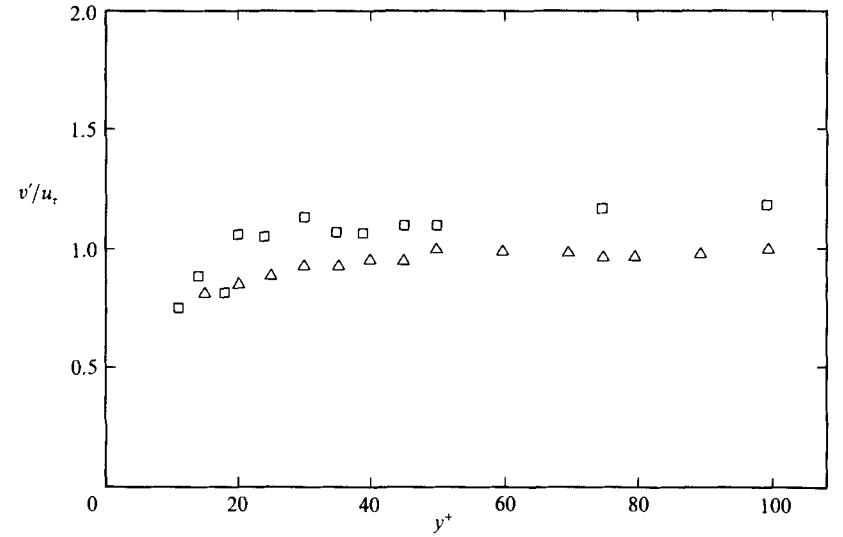

FIGURE 5. Comparison of root mean square of velocity fluctuations normal to wall: □, water; △, EWS drag-reducing flow.

to the u' results, the peak values of v' for both of the drag-reducing flows are lower than the peak r.m.s. value for the water flow. These results are consistent with those of Logan (1972) in trend although the levels measured here differ substantially from Logan's square-channel measurements.

The turbulent-shear-stress distributions across the channel half-height are shown in figure 6 for the flows with equal wall shear stress. For the drag-reducing flow, the normalized turbulent shear stress in the outer portion of the flow is the same as that of the water flow. However, as the wall is approached, the $\overline{uv}$ profile of the drag-reducing flow has a broader peak and the peak region occurs farther away from the wall than for the water flow. Similar results (see Luchik 1985) were obtained in the comparison for the drag-reducing flow and water flow at equal Reynolds numbers.

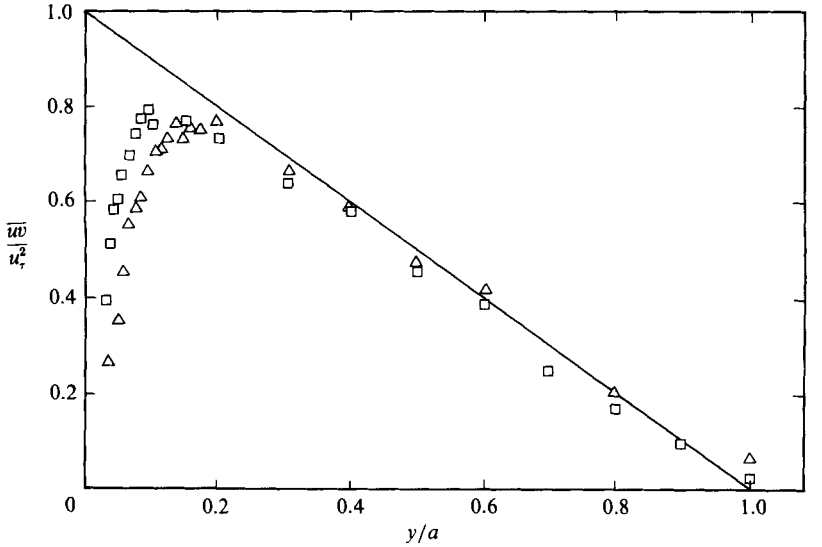

FIGURE 6. Comparison of Reynolds-stress profiles: □, water; △, EWS drag-reducing flow.

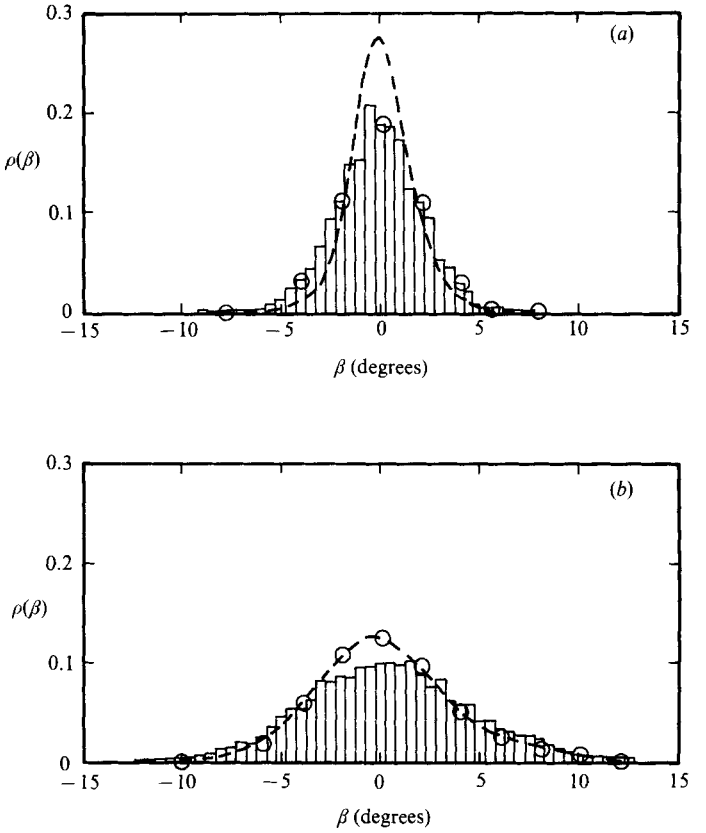

FIGURE 7. Distribution of instantaneous flow angle for the water flow: (*a*) centreline of channel; (*b*) $y^+ = 50$. ---, Alfredsson & Johansson (1984); ○, Kreplin & Eckelmann (1979).

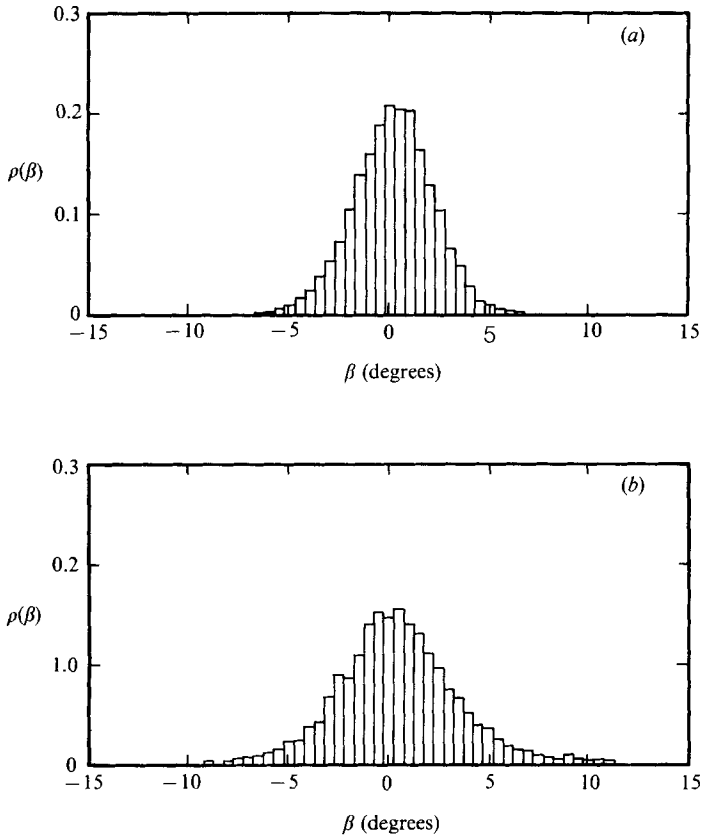

FIGURE 8. Distribution of instantaneous flow angle for the ERN drag-reducing flow: (*a*) centreline of channel; (*b*) $y^+ = 50$.

The instantaneous flow angle for these fully developed channel flows is given by

$$\beta = \tan^{-1}\frac{V}{U}, \tag{3.1}$$

where V is the instantaneous velocity component normal to the wall and U is the instantaneous streamwise velocity component. This information is useful because in a fully developed flow the flow angle shows whether fluid is moving away from or toward the wall and thus the extent and magnitude of large values for β are good measures of the amount of turbulent mixing.

Figure 7 shows the instantaneous-flow-angle distributions for the water flow at two y-locations. The X-wire data of Alfredsson & Johansson (1984) and Kreplin & Eckelmann (1979) are also shown on this figure. As expected, the water data show a broadening of the distribution of the instantaneous flow angle and a decrease in the peak probability density as the wall is approached. The flow-angle distributions for cases ERN and EWS on the channel centreline and at $y^+ = 50$ are shown in figures 8 and 9 respectively. On the channel centreline there is very little difference in flow-angle distributions for the water flow and drag-reducing flows. This, along with previous mean statistics, indicates that there is very little change in the turbulence in this region of the flow and further supports the view that the polymers need not be in the outer portion of the flow for drag reduction to occur. However, at

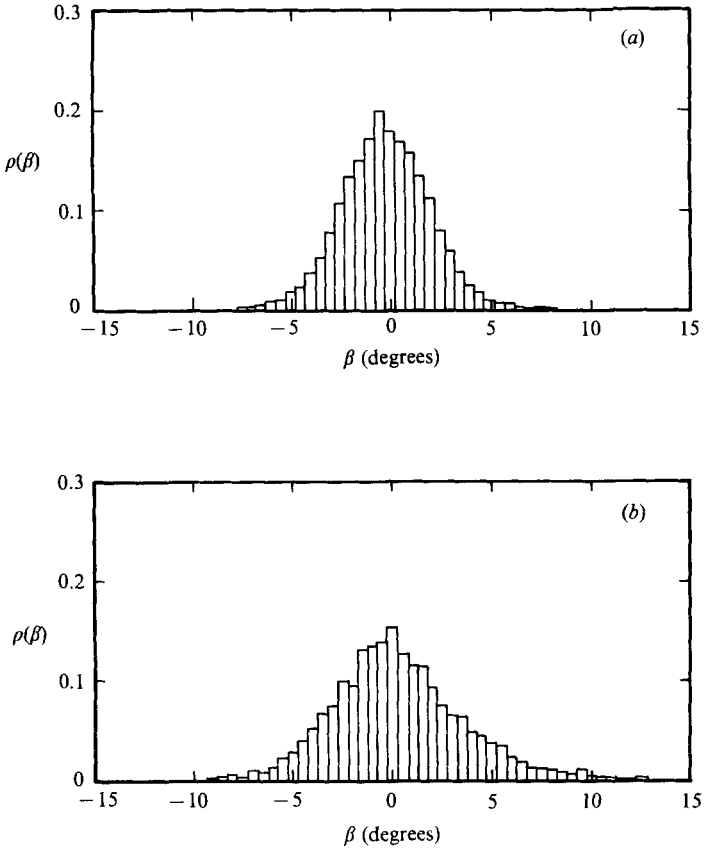

FIGURE 9. Distribution of instantaneous flow angle for the EWS drag-reducing flow: (*a*) centreline of channel; (*b*) $y^+ = 50$.

$y^+ = 50$ there is a notable increase in the probability of an occurrence of a flow angle near zero for the drag-reducing flows. This result is consistent with the decrease in the r.m.s. of the normal velocity and damping of the turbulent structure in this portion of the flow. At $y^+ \approx 10$, the flow-angle distributions for each of the three flow situations become similar. All of this information supports the view that the polymer solutions must reside in the buffer region to achieve drag reduction.

4. Turbulent-structure results

Several methods have been proposed to detect the burst or ejection structure using Eulerian velocity information. Luchik & Tiederman (1987) have shown that a modified u-level technique coupled with a grouping parameter yielded a good estimate of both the average time between bursts and conditional averages of the turbulent velocity signals for ejection events. This technique defines the leading edge of an ejection when

$$u < -Lu', \tag{4.1}$$

and the trailing edge of an ejection when

$$u \geqslant -0.25\,Lu'. \tag{4.2}$$

The threshold level L is defined by

$$L = \frac{|\bar{u}_2|}{u'}, \tag{4.3}$$

where $\bar{u}_2$ is the average of the streamwise fluctuation when $u < 0$ and $v > 0$. With this technique ejection detections are grouped into burst detections using a grouping parameter τ_E, which is the maximum time between ejections from the same burst. This parameter is determined from the distribution of the time between ejections, as described by Luchik & Tiederman (1987). It is important to note that for all three flows there was a threshold-level range of approximately $0.75 \leqslant L \leqslant 1.25$ over which the number of bursts detected was constant. In all three cases the value of L given by (4.3) was approximately 1.0 and in the middle of the range of threshold independence for the detection of bursts. The structural results which are reported later in this section were all deduced using the value of L from (4.3) that is believed to be the optimal level for detecting ejection- and burst-related phenomena.

The location normal to the wall for these measurements is important. Below $y^+ \approx 5$, dye-slot flow visualization reveals the streaky structure because the velocity field in the linear sublayer is not disturbed significantly by the ejected fluid (see Tiederman *et al.* 1985). Slow-speed fluid from a streak must be lifted to $y^+ \gtrsim 10$ before it is entrained in burst events in Newtonian fluids (see Kline *et al.* 1967). As shown by Bogard & Tiederman (1986), the number of detections per burst increases substantially for $15 < y^+ < 100$ as the interface of the ejected fluid becomes more convoluted. Near the channel's centreline, burst events from the opposite wall will be detected. As a result there is some minimum distance from the wall where all burst events and only burst events from one wall are detected most easily with a velocity probe. Since the near-wall region is thicker in the drag-reducing flows, the location of $y^+ = 30$ was chosen as the detection location for all three flows in this study.

4.1. *Average time between bursts*

Figure 10 shows the variation in the average time between bursts with percentage drag reduction for low-concentration drag-reducing flows. The average time between bursts in the drag-reducing flows has been normalized with the average time between bursts of a water flow at an equal shear velocity. These results show that there is good agreement between the modified u-level results and the flow-visualization results. Also, note that the ratio of burst period in the 31% drag-reducing flow to a water flow at an equal shear velocity is equal to 1.67. This ratio is essentially the same as the ratio of the streak spacing in the same two flows, which is 1.58 (see Oldaker & Tiederman 1977). A similar result occurs for the 22% drag-reducing flow, as shown on figure 10 where the ratio of $\bar{T}_B$ is compared to λ^+. Thus, the burst rate from a streak for the well-mixed, low-concentration, drag-reducing flows is equal to that for a Newtonian flow.

This result does not necessarily contradict the findings of Luchik & Tiederman (1984), Tiederman *et al.* (1985) or McComb & Rabie (1982), who all noted that the change in burst period was greater than the change in streak spacing for drag-reducing flows with wall-layer polymer concentration larger than 20 p.p.m. For these higher-concentration wall regions there may be some damping of relatively large-scale structures. In contrast, the 1–2 p.p.m. flows of this study achieve drag reduction through damping of only the smaller (low-amplitude or weaker) turbulent eddies.

Direct demonstration that only the smaller-amplitude eddies were damped is given in figures 11 and 12 where the probability density for the frequency of

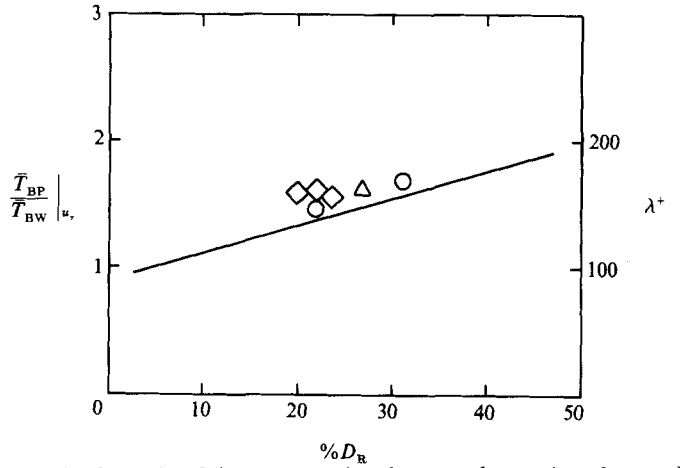

FIGURE 10. Variation in the ratio of the average time between bursts in a drag-reducing flow to the average time between bursts in a water flow at an equal shear velocity: ◇, flow visualization – present study; ○, modified u-level – present study; △, flow visualization – Walker *et al.* (1985); ——, $\lambda^+ = 99.7 + 1.9\,D_R$.

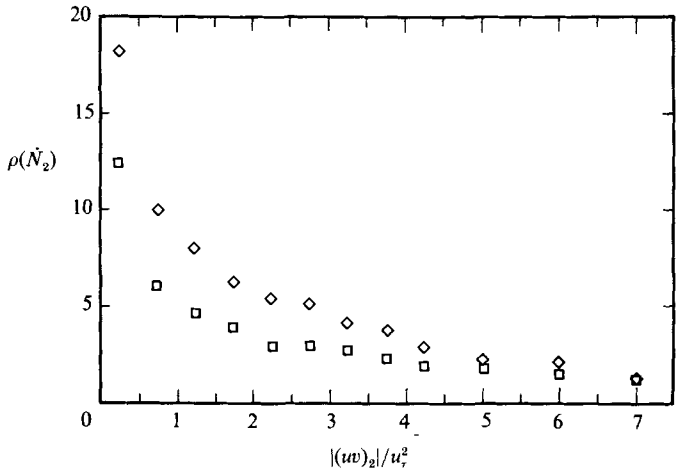

FIGURE 11. Comparison of the probability density for the rate of occurrence of quadrant 2 events as a function of threshold: ◇, water flow; □, EWS drag-reducing flow.

occurrence of quadrant 2 ($u < 0$ and $v > 0$) and quadrant 4 ($u > 0$ and $v < 0$) events are shown as a function of a threshold parameter

$$h_i = (uv)_i/u_\tau^2. \tag{4.4}$$

The comparison is presented for only the equal-wall-shear-stress flows because in this case the dimensional distance from the wall and the dimensional timescale, as well as the non-dimensional distance ($y^+ = 30$) and non-dimensional timescale, are equal. A direct comparison at the same physical location is most easily understood because the time-averaged statistics of the velocity signals as a function of y^+ differ in the drag-reducing flows compared to the water flow. At low threshold values it is clear that the probability density of both quadrant 2 and quadrant 4 events are decreased substantially. The probability density of high-threshold quadrant 2 events is unchanged and there is a small increase in the probability density of quadrant 4 events for

$$4.5 \leqslant h_4 \leqslant 6.5. \tag{4.5}$$

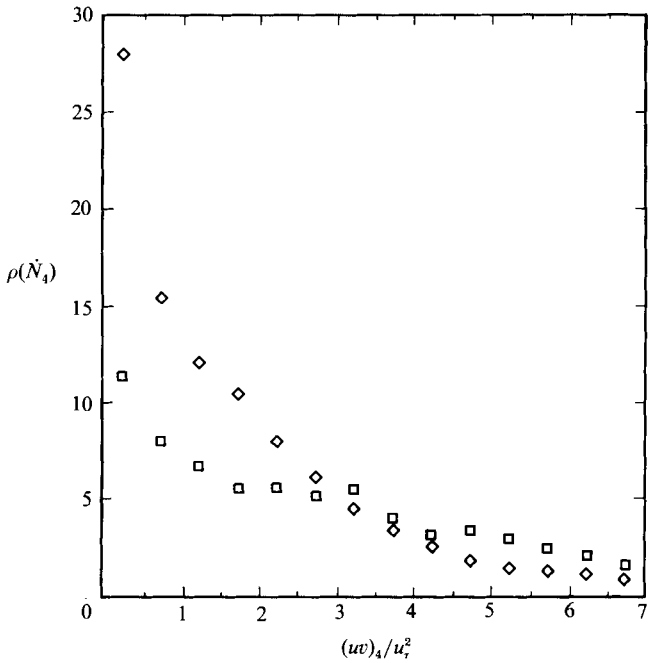

FIGURE 12. Comparison of the probability density for the rate of occurrence of quadrant 4 events as a function of threshold: ◇, water flow; □, EWS drag-reducing flow.

This increase in high-threshold quadrant 4 events is consistent with the larger streamwise velocity in the turbulent core of the drag-reducing flow. Please note that at this point these quadrant 2 and quadrant 4 motions have not been associated with bursts or ejections and sweeps. As shown by Board & Tiederman (1986) there is a high correlation between quadrant 2 events and ejection events at high thresholds. However at the lower thresholds where the damping is largest there is not a good correlation between quadrant 2 events and an ejection, and by implication, quadrant 4 events and sweeps. It should be noted that similar damping of quadrant 2 events occurred in a comparison of the ERN drag-reducing flow with the water flow.

4.2. *Burst characteristics*

Figures 13 and 14 show conditionally averaged signals for the velocity fluctuations and the uv product centred on the leading and trailing edges of burst events for the equal-shear-stress flows. As shown by Bogard & Tiederman (1987), phase scrambling or loss of coherence occurs for times displaced from the condition used to centre these types of average. This scrambling is due to variations in the burst-event strength and size as well as the spanwise location of the probe relative to the 'centreline' of the event. In this study, the conditionally averaged signals for $|T^+| \leqslant 10$ are representative of signals from individual bursts. The shear velocity was used to normalize the signals in figures 13 and 14 because u_τ is the same for both flows and the reader can readily identify the differences and similarities in the conditionally averaged signals. The usual normalization with r.m.s. levels is not as useful because, at $y^+ = 30$, u' and v' are not the same for the two flows.

Figure 13 shows there is a larger decrease in $\langle u \rangle$ associated with the leading edge of a burst in the drag-reducing flow, while the increase in $\langle v \rangle$ is slightly smaller and

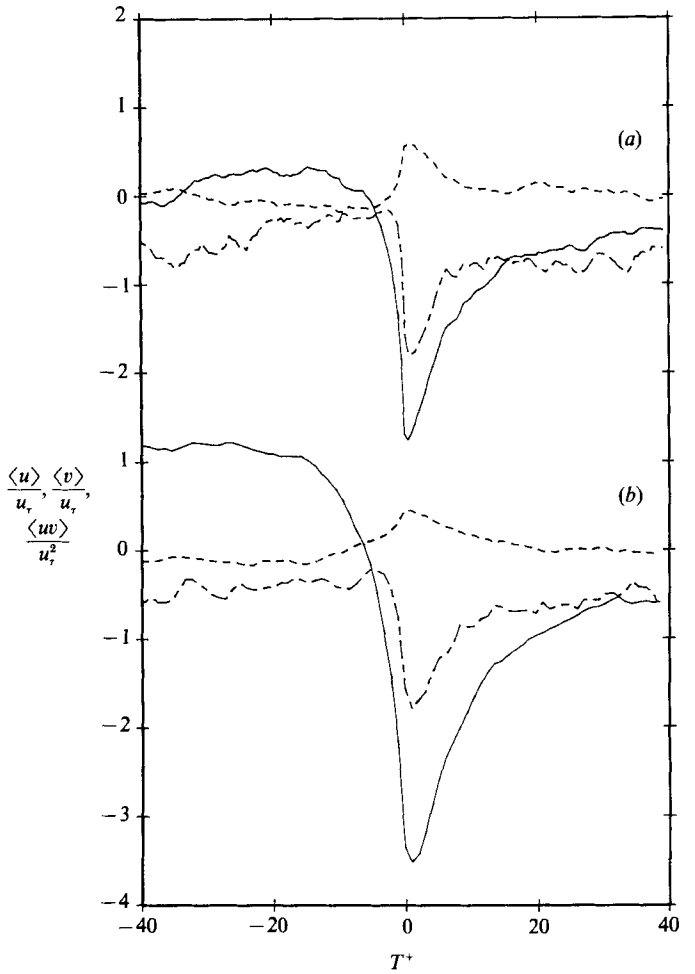

FIGURE 13. Conditionally averaged signals aligned at the leading edge of a burst: (*a*) water; (*b*) EWS drag-reducing flow. ——, $\langle u\rangle/u_\tau$; – – –, $\langle v\rangle/u_\tau$; —·—, $\langle uv\rangle/u_\tau^2$.

the $\langle uv\rangle$ signal is unchanged. The larger change in $\langle u\rangle$ yields a well-defined leading edge for the burst events. This is consistent with the view from dye-slot flow visualization where the ejections and bursts were visibly more clearly defined in drag-reducing flows (see Luchik & Tiederman 1984). The other significant feature is that $\langle u\rangle$ is positive (larger than the local mean) prior to the burst in the drag-reducing flow while the average level prior to the burst in the water flow is zero.

At the trailing edge, again the largest difference occurs in the magnitude of the increase in $\langle u\rangle$ and the positive value of $\langle u\rangle$ following the burst in the drag-reducing flow. As before, the increase in the $\langle v\rangle$ signal is only slightly smaller for events in the drag-reducing flow. Note that in both flows there is a sharper gradient in $\langle u\rangle$ at the trailing edge of the burst, which is consistent with previous results (see Bogard & Tiederman 1987).

The larger variation in $\langle u\rangle$ at both the leading and trailing edge of the burst is consistent with the larger gradient in the time-averaged streamwise velocity ($\mathrm{d}\bar{U}/\mathrm{d}y$) at $y^+ = 30$ in the drag-reducing flow. It should also be noted that if u' had been used to normalize $\langle u\rangle$, the non-dimensional variation of $\langle u\rangle/u'$ would decrease and

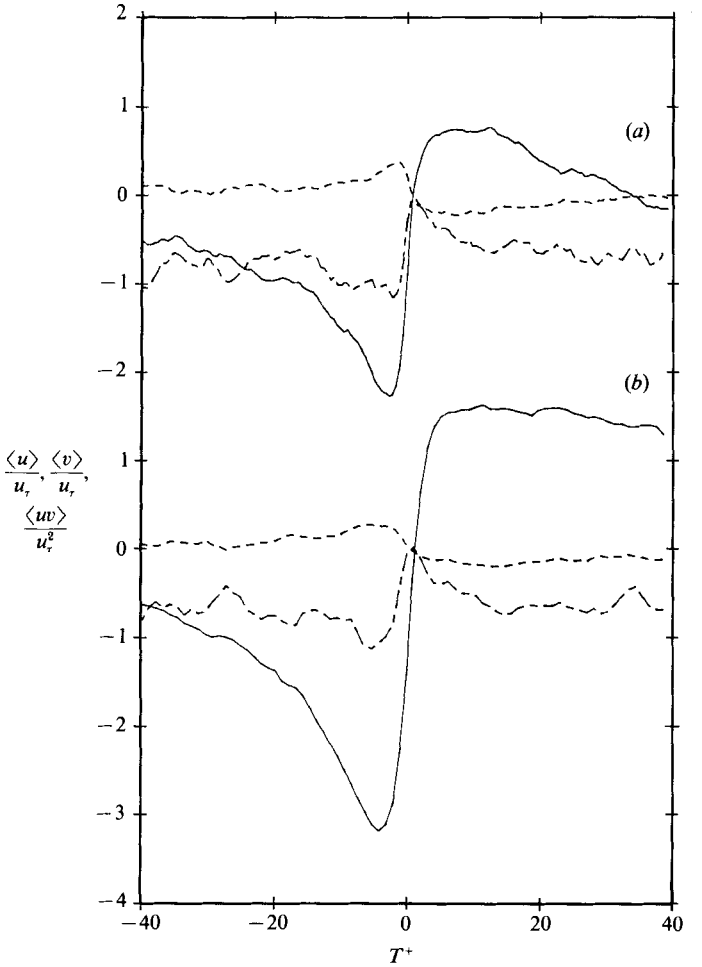

FIGURE 14. Conditionally averaged signals aligned at the trailing edge of a burst: (*a*) water; (*b*) EWS drag-reducing flow. ——, $\langle v\rangle/u_\tau$; – – –, $\langle v\rangle/u_\tau$; —·—, $\langle uv\rangle/u_\tau^2$.

obscure the variation in $\langle u\rangle$ because, at $y^+ = 30$, u' is larger in the drag-reducing flow (see figure 3).

In comparing figures 13 and 14 it is clear that a larger $\langle uv\rangle$ minimum and a larger $\langle v\rangle$ maximum are associated with the leading edge of bursts in both flows than with the trailing edge. A similar result was obtained by Bogard & Tiederman (1987) at $y^+ = 15$ for a lower-Reynolds-number water flow. It is consistent to conclude that on average the quadrant 2 signal of the first ejection of a Newtonian and a drag-reducing burst will be larger than the quadrant 2 signal from the succeeding ejections of a multiple-ejection burst.

While it is important to emphasize the differences in the structural events when drag reduction occurs, it is also important to note that the basic character of the velocity signatures associated with a burst are unchanged. This is also true for the ERN drag-reducing flow (see Luchik 1985) and shows that drag reduction is achieved by modifying the burst event and not by eliminating all burst-type motions from the flow.

A comparison of several other conditionally sampled quantities during burst

	Quadrant	Water	ERN	EWS
Re_h	—	17800	17800	22000
% D_R	—	0	22	31
$\bar{T}_B$ (s)	—	0.063	0.106	0.105
Average number of ejections/burst	—	2.1	2.3	2.5
$\bar{T}_D$ (s)	—	0.024	0.041	0.045
$\bar{T}_D^+$	—	37.6	50.0	70.5
Intermittency = $\bar{T}_D/\bar{T}_B$	—	0.38	0.39	0.43
Percentage contribution during a burst to uv in quadrant i	1	7	9	14
	2	89	90	90
	3	76	83	88
	4	7	8	11
Percentage contribution during a burst to $\overline{uv}$ from each quadrant	1	−2	−3	−4
	2	88	84	96
	3	−29	−29	−48
	4	5	5	8
	Sum	62	57	52

TABLE 3. Comparison of conditionally sampled quantities during a burst detection for the three flows using the modified u-level technique at $y^+ = 30$

detections for the three flows is given in table 3. The purpose of these comparisons is to deduce how the drag-reducing additives have affected the principal event associated with momentum transport between the wall region and the outer, core region of the channel flow. In addition to the average time between bursts the parameters chosen for comparison are: (i) the average duration of the burst, which is given by

$$\bar{T}_D = \frac{1}{N_D} \Sigma (T_D)_i, \tag{4.6}$$

where N_D is the number of detections and $(T_D)_i$ is the duration of the ith event; (ii) the percentage contribution of uv in a given quadrant (in u, v-coordinates) during all bursts to the total uv in that quadrant, which is given by

$$100 \times \frac{\int_0^T uv(t)\, \delta(t)\, \sigma_i(t)\, \mathrm{d}t}{\int_0^T uv(t)\, \sigma_i(t)\, \mathrm{d}t}, \tag{4.7}$$

where $\delta(t)$ is one during a burst detection and zero otherwise. Similarly, $\sigma_i(t)$ is one when the uv product is in quadrant i and zero otherwise; (iii) the percentage contribution to the time-averaged value of uv from each quadrant during a burst, given by

$$\frac{100 \times \int_0^T uv(t)\, \delta(t)\, \sigma_i(t)\, \mathrm{d}t}{\int_0^T uv(t)\, \mathrm{d}t}. \tag{4.8}$$

From table 3 it can be seen that the modified u-level technique yields values for the average number of ejections per burst that are in good agreement with those obtained using flow visualization. The duration of a burst increases in the drag-

	Water		EWS	
	ejection	burst	ejection	burst
$\langle u \rangle / u_\tau$	−2.85	−2.01	−3.55	−2.08
$\langle v \rangle / u_\tau$	0.451	0.276	0.266	0.151
$\langle uv \rangle / u_\tau^2$	−1.60	−1.17	−0.968	−0.677

TABLE 4. Conditionally averaged signal levels during an ejection and a burst at $y^+ = 30$

reducing flows in a manner similar to the increase for the time between bursts. As a result the intermittency for the burst is almost the same for all three flows.

The contributions to uv in a given quadrant during a burst detection are much larger than the intermittency values for quadrants 2 and 3 and much smaller than the intermittency values for quadrants 1 and 4. (Note that the contribution to uv in each quadrant would be equal to the intermittency value if there is no correlation between a detection and uv.) This result is in qualitative agreement with Bogard & Tiederman's (1987) result for ejections based on time periods when dye-marked ejections were in contact with their hot-wire probe at $y^+ = 15$ and shows that burst events are correlated with quadrant 2- and quadrant 3-type motions.

The contribution to $\overline{uv}$ from each quadrant during a burst event is very similar for the water flow and equal-Reynolds-number flow. There is somewhat more quadrant 3 turbulent momentum transfer for the equal-wall-shear flow. In all three flows the total contribution to $\overline{uv}$ from all four quadrants during a burst is significantly larger than the intermittent value, but it does decrease as the amount of drag reduction increases. The implication of this decrease is that the contribution of sweeps to $\overline{uv}$ increases. The shape of the mean velocity profile in the drag-reducing flows is consistent with this hypothesis.

Table 4 shows how the conditionally averaged signals at $y^+ = 30$ ($y = 0.722$ mm) compare for the water flow and the drag-reducing flow at equal wall shear stress. Comparisons are not presented for the equal-Reynolds-number flow because changes in the normalized profiles of the time-averaged statistics confuse the interpretation of the results. That is, there is nothing unique about $y^+ = 30$ for the equal-Reynolds-number flows. For the equal-wall-shear flows, the physical distance from the wall is the same and the comparisons and interpretations on that basis are clear.

There are a number of general characteristics that should be noted. For example the average negative value of $\langle u \rangle$ during an ejection in both flows is very similar to the respective minimums of $\langle u \rangle$ shown in figures 13 and 14. This agreement is not unexpected since the minimum levels centred on the leading and trailing edge of a burst (first and last ejection of a burst) for the water flow are very similar, as are the respective minimums for the EWS drag-reducing flow. After accounting for the phase jitter that reduces signal levels in figures 13 and 14 for $|T^+| \geqslant 10$, one should expect average levels for $\langle u \rangle$ that correspond closely to the average of the respective minimum peaks. Similarly the average values of $\langle v \rangle$ and $\langle uv \rangle$ during an ejection are close to the average of the extreme levels of those signals in figures 13 and 14. Finally, since a burst may contain two or more ejections each separated (from an Eulerian viewpoint) by non-ejecting signals, the average values for $\langle u \rangle$, $\langle v \rangle$ and $\langle -uv \rangle$ are smaller during the bursts than during the ejections.

Based on the damping seen previously for v', $-\overline{uv}$, as well as quadrant 2 and quadrant 4 events, it is not surprising to see that $\langle v \rangle$ decreases by 41% during an

ejection and by 45% during a burst in the drag-reducing flow. Similarly the absolute value of $\langle uv \rangle$ decreases by 42% during an ejection and 40% during a burst in the drag-reducing flow. These decreases are much larger than those for v' and $|\overline{uv}|$, which suggests that the polymer additive has a substantial effect on the burst events, particularly the lower-threshold events considering figure 11 and that portion of the event well after the leading edge considering figures 13 and 14.

The rather large increase in the negative value for $\langle u \rangle$ during an ejection in a drag-reducing flow supports the view that large quadrant 2 events in the drag-reducing flow result from very low-speed fluid moving outward with a rather ordinary (for an ejection) normal velocity component. This difference for the $\langle u \rangle$ signals during an ejection are probably more significant than the equal levels of $\langle u \rangle$ during a burst. Since the latter includes more averaging, the equivalent levels of $\langle u \rangle$ during a burst may be coincidental.

5. Conclusions

A comparison of the long-time-averaged as well as the conditionally averaged flow quantities of a drag-reducing flow with a water flow showed that the decrease in wall shear stress in low-concentration polymer flows is associated with damping of the velocity fluctuations normal to the wall. The turbulent shear stress is also damped in this region ($y^+ \leqslant 60$) indicating a decrease in turbulent mixing of the fluid near the wall with fluid in the outer portion of the flow. Instantaneous flow-angle distributions for the water and two drag-reducing flows indicated that the flow on the centreline of the channel is very similar. However, in the buffer region, the drag-reducing flows have a narrower distribution of flow angle than a water flow with a higher probability for angles $-0.25° \leqslant \beta \leqslant 0.25°$ in these drag-reducing flows. This is further evidence of decreased mixing.

In the low-concentration drag-reducing flows the average time between bursts increased, which is consistent with the damping of the turbulent shear stress near the wall. However, the change in the average time between bursts for the low-concentration drag-reducing flow, when compared to a water flow at the same wall shear stress, was equal to the change in streak spacing. Thus, the average time between bursts from a streak in the low-concentration drag-reducing flows was the same as that for a water flow. The average number of ejections per burst was 2.3–2.5 for the low-concentration, well-mixed solutions. Further upstream near the injector, where the additive concentration is about 20 p.p.m. or more and not yet uniform, the average number of ejections per burst is about 3.5 (Luchik & Tiederman 1984). This difference and the differences in the time between bursts for the same level of drag reduction indicate that either the mechanism by which a well-mixed, very low concentration (1–2 p.p.m.) of additives reduces drag is different to the mechanism for flows with wall-layer concentrations above 20–50 p.p.m. or that the evolving concentration profiles produce flows where the turbulent mechanisms have not yet reached an equilibrium state.

Although the average time between bursts from a streak was the same in the low-concentration drag-reducing flow as in a water flow with the same shear velocity, the conditionally averaged velocity signatures of the burst structures differed in significant ways. In the presence of the drag-reducing solution, the smaller-scale turbulence was damped most. Thus the conditionally averaged signals in a drag-reducing flow had a much larger negative $\langle u \rangle$ peak while $\langle v \rangle$ remained essentially unchanged at both the leading and trailing edge of the burst. Sweep-like signatures

were seen at both the leading and trailing edge of the burst and the sweep–burst and burst–sweep interfaces were more clearly defined in the drag-reducing flows.

All of the results presented here show that drag reduction was achieved through damping of the lower-threshold turbulent motions as well as those transport motions following the leading edge of a burst. Higher-threshold motions were not damped. Although the conditionally averaged signals changed, the basic character of the burst event is unchanged in drag-reducing flows. It is likely that the conformation of the additive molecules and the turbulent motions in the flow achieve an equilibrium state where some strong turbulent stretching is required to keep the molecules extended so that lower-threshold turbulence can be damped by viscoelastic properties of the dilute polymer solution.

This research was supported by the Office of Naval Research contract number NOOO14-83K-0183, NRO62-54. The assistance of C. David Bustetter and David T. Walker in analysing data is gratefully acknowledged.

REFERENCES

ACHIA, B. U. & THOMPSON, D. W. 1977 Structure of the turbulent boundary layer in drag reducing pipe flow. *J. Fluid Mech.* **81**, 439.

ALFREDSSON, P. H. & JOHANSSON, A. V. 1984 On the detection of turbulence generating events. *J. Fluid Mech.* **139**, 325.

BERMAN, N. S. 1986 Velocity fluctuations in non-homogeneous drag reduction. *Chem. Engng Commun.* **42**, 37.

BEWERSDORFF, H.-W. 1985 Heterogeneous drag reduction in turbulent pipe flow. In *The Influence of Polymer Additives on Velocity and Temperature Fields* (ed. B. Gampert), p. 337. Springer.

BOGARD, D. G. 1982 Investigation of burst structures in turbulent channel flows through simultaneous flow visualization and velocity measurements. Ph.D. thesis, Purdue University.

BOGARD, D. G. & TIEDERMAN, W. G. 1983 Investigation of flow visualization techniques for detecting turbulent bursts. In *Symposium on Turbulence, 1981* (ed. X. B. Reed, G. K. Patterson & J. L. Zakin), p. 289. University of Missouri – Rolla.

BOGARD, D. G. & TIEDERMAN, W. G. 1986 Burst detection with single-point velocity measurements. *J. Fluid Mech.* **162**, 389.

BOGARD, D. G. & TIEDERMAN, W. G. 1987 Characteristics of ejections in turbulent channel flow. *J. Fluid Mech.* **179**, 1.

CORINO, E. R. & BRODKEY, R. S. 1969 A visual study of turbulent shear flow. *J. Fluid Mech.* **37**, 1.

DONOHUE, G. L., TIEDERMAN, W. G. & REISCHMAN, M. M. 1972 Flow visualization of the near-wall region in a drag-reducing flow. *J. Fluid Mech.* **56**, 559.

FRINGS, B. 1985 Annular injection of concentrated polymer solutions into the wall region of a turbulent pipe flow. In *The Influence of Polymer Additives on Velocity and Temperature Fields* (ed. B. Gampert), p. 337. Springer.

Instruction Manual for System 9100-6, Single Channel High Power LDV. Thermo-Systems Incorporated, St Paul, Minnesota.

JOHANSSON, A. V. & ALFREDSSON, P. H. 1983 Effects of imperfect spatial resolution on measurements of wall-bounded turbulent shear flows. *J. Fluid Mech.* **137**, 409.

KIM, H. T., KLINE, S. J. & REYNOLDS, W. C. 1971 The production of turbulence near a smooth wall in a turbulent boundary layer. *J. Fluid Mech.* **50**, 133.

KLINE, S. J., REYNOLDS, W. C., SCHRAUB, F. A. & RUNSTADLER, P. W. 1967 The structure of turbulent boundary layers. *J. Fluid Mech.* **30**, 741.

KREPLIN, H.-P. & ECKELMANN, H. 1979 Instantaneous direction of the velocity vector in a fully developed turbulent channel flow. *Phys. Fluids* **22**, 1210.

LOGAN, S. E. 1972 A laser velocimeter measurement of Reynolds stress in dilute polymer solutions. Ph.D. thesis, California Institute of Technology.

LUCHIK, T. S. 1982 A laser velocimeter investigation of turbulent flow in an axisymmetric sudden expansion. Master's thesis, Purdue University.

LUCHIK, T. S. 1985 The effect of drag-reducing additives on the turbulent structure in channel flows. Ph.D. thesis, Purdue University.

LUCHIK, T. S. & TIEDERMAN, W. G. 1984 Bursting rates in channel flows and drag reducing channel flows. In *Symposium on Turbulence, 1983* (ed. X. B. Reed, G. K. Patterson & J. L. Zakin), p. 15. University of Missouri – Rolla.

LUCHIK, T. S. & TIEDERMAN, W. G. 1985 Effect of spanwise probe volume length on laser velocimeter measurements in wall bounded turbulent flows. *Exp. Fluids* **3**, 339.

LUCHIK, T. S. & TIEDERMAN, W. G. 1987 Timescale and structure of ejections and burst in turbulent channel flows. *J. Fluid Mech.* **174**, 529.

MCCOMB, W. D. & RABIE, L. H. 1982 Local drag reduction due to injection of polymer solutions into turbulent flow in a pipe. Part I: Dependence on local polymer concentration; Part II: Laser-Doppler measurements of turbulent structure. *AIChE J.* **28**, 547.

OFFEN, G. R. & KLINE, S. J. 1975 A comparison and analysis of detection methods for the measurement of production in a boundary layer. In *Proc. 3rd Biennial Symposium on Turbulence in Liquids* (ed. G. K. Patterson & J. L. Zakin), p. 289. University of Missouri – Rolla.

OLDAKER, D. K. & TIEDERMAN, W. G. 1977 Spatial structure of the viscous sublayer in drag-reducing channel flows. *Phys. Fluids Suppl.* **20**, S133.

REISCHMAN, M. M. & TIEDERMAN, W. G. 1975 Laser-Doppler anemometer measurements in drag-reducing channel flows. *J. Fluid Mech.* **70**, 369.

STEVENSON, W. H., THOMPSON, H. D. & ROESLER, T. C. 1982 Direct measurements of laser velocimeter bias errors in a turbulent flow. *AIAA J.* **20**, 1720.

TIEDERMAN, W. G., LUCHIK, T. S. & BOGARD, D. G. 1985 Wall layer structure and drag reduction *J. Fluid Mech.* **156**, 419.

TIEDERMAN, W. G., SMITH, A. J. & OLDAKER, D. K. 1977 Structure of the viscous sublayer in drag-reducing channel flows. In *Turbulence in Liquids, 1975* (ed. J. L. Zakin & G. K. Patterson), p. 312. University of Missouri – Rolla.

WALKER, D. T., TIEDERMAN, W. G. & LUCHIK, T. S. 1986 Optimization of the injection process for drag reducing additives. *Exp Fluids* **4**, 114.

WELLS, C. S. & SPANGLER, J. G. 1967 Injection of a drag-reducing fluid into turbulent pipe flow of a Newtonian fluid. *Phys. Fluids* **10**, 1980.

WILLMARTH, W. W. & SHARMA, L. K. 1984 Study of turbulent structure with hot wires smaller than the viscous length. *J. Fluid Mech.* **142**, 121.

WU, T. Y. & TULIN, M. P. 1972 Drag reduction by ejecting additive solutions into a pure water boundary layer. *Trans. ASME D: J. basic Engng* **74**, 749.